AD-A077 886 INDIANA UNIV AT BLOOMINGTON DEPT OF CHEMISTRY F/G 7/4
EVALUATION OF CLASSICAL VAPORIZATION AND IONIZATION INTERFERENC--ETC(U)
NOV 79 R N SAVAGE , G M HIEFTJE N00014-76-C-0838
UNCLASSIFIED 29 NL

| OF |
ADA 077886

END
DATE FILMED
1 -80
DDC

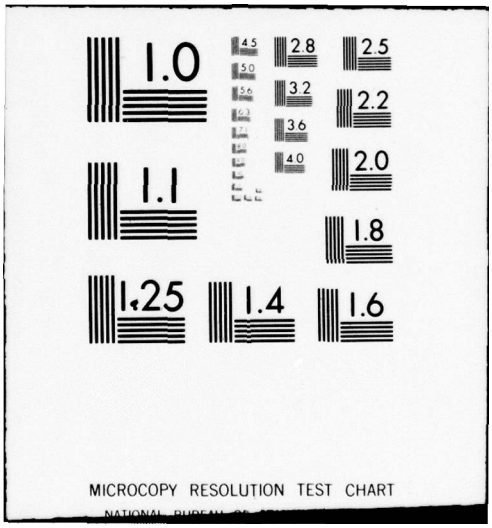
1.0
1.1
1.25
1.4
1.6
1.8
2.0
2.2
2.5
2.8
3.2
3.6
4.0
4.5
5.0
5.6
6.3
MICROCOPY RESOLUTION TEST CHART

UNCLASSIFIED
SECURITY CLASSIFICATION OF THIS PAGE (When Data Entered)

LEVEL II

REPORT DOCUMENTATION PAGE

1. REPORT NUMBER: TWENTY-THREE	2. GOVT ACCESSION NO.
3. RECIPIENT'S CATALOG NUMBER	
4. TITLE (and Subtitle): Evaluation of Classical Vaporization and Ionization Interferences in a Miniature ICP	5. TYPE OF REPORT & PERIOD COVERED: Interim Technical Report
	6. PERFORMING ORG. REPORT NUMBER: 29
7. AUTHOR(s): R. N. Savage and G. M. Hieftje	8. CONTRACT OR GRANT NUMBER(s): N-14-76-C-0838
9. PERFORMING ORGANIZATION NAME AND ADDRESS: Department of Chemistry, Indiana University, Bloomington, IN 47405	10. PROGRAM ELEMENT, PROJECT, TASK AREA & WORK UNIT NUMBERS: NR 051-622
11. CONTROLLING OFFICE NAME AND ADDRESS: Office of Naval Research, Washington, D. C.	12. REPORT DATE: November 30, 1979
	13. NUMBER OF PAGES: 39
14. MONITORING AGENCY NAME & ADDRESS (if different from Controlling Office)	15. SECURITY CLASS. (of this report): UNCLASSIFIED
	15a. DECLASSIFICATION/DOWNGRADING SCHEDULE

16. DISTRIBUTION STATEMENT (of this Report)

Approved for public release; distribution unlimited

17. DISTRIBUTION STATEMENT (of the abstract entered in Block 20, if different from Report)

DDC RECEIVED DEC 11 1979 A

18. SUPPLEMENTARY NOTES

Prepared for publication in ANALYTICAL CHEMISTRY

19. KEY WORDS (Continue on reverse side if necessary and identify by block number)

Inductively coupled plasma, emission spectroscopy, multielement analysis, matrix effects, interferences

20. ABSTRACT (Continue on reverse side if necessary and identify by block number)

The magnitude of several classical interelement interferences in a miniature ICP is found to be small but dependent on experimental conditions. The origin and manifestation of these interference (matrix) effects are shown to be complex and influenced most strongly by: 1) observation window in the plasma's tail flame, 2) rf power, and 3) nebulizer gas flow rate. In particular, vaporization interference matrices (Al and PO_4) caused a depression in the intensities of both the neutral atom and ion lines of Ca with the Ca II

DD FORM 1 JAN 73 1473 EDITION OF 1 NOV 65 IS OBSOLETE S/N 0102-014-6601 | UNCLASSIFIED
SECURITY CLASSIFICATION OF THIS PAGE (When Data Entered)

AD A077886

DDC FILE COPY

79 12 7 053

20. (continued)

line experiencing a larger effect than that of Ca I. Conversely, easily ionized elements (such as Na and Cs) enhanced both Ca and Mg neutral atom and ion line intensities, with the atom lines exhibiting a larger increase than those of the ions. Because both the neutral atom and ion lines of Ca and Mg are enhanced by Na and Cs, and to identical degrees, a simple shift in ionization equilibria seems not to produce the observed interference. Clearly, more fundamental knowledge concerning the formation and excitation of atoms in ICP sources is needed before interference mechanisms can be elucidated. However, with the information gained from the present study, compromise conditions for simultaneous multielement analysis can be selected which provide interference levels that are minimal for most, but not all, analyte-matrix combinations and are comparable to those found in conventional ICP sources.

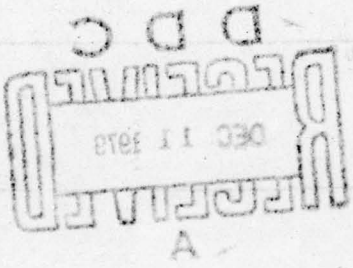

OFFICE OF NAVAL RESEARCH

Contract N14-76-C-0838

Task No. NR 051-622

(9) TECHNICAL REPORT NO. 23

(6) EVALUATION OF CLASSICAL VAPORIZATION AND IONIZATION INTERFERENCES IN A MINIATURE ICP

by

(10) R. N. Savage and G. M. Hieftje

(14) 29

(15) N000 14-76-C-0838

Prepared for Publication

in

ANALYTICAL CHEMISTRY

Indiana University

Department of Chemistry

Bloomington, Indiana 47405

(11) November 1979

(12) 42

176 685

B

Evaluation of Classical Vaporization and Ionization Interferences in a Miniature ICP

R. N. Savage[a] and G. M. Hieftje*

Department of Chemistry

Indiana University

Bloomington, IN 47405

*Author to whom correspondence should be addressed

[a]Current address: Instrumentation Laboratories, Inc., Wilmington, MA 01887

BRIEF

Vaporization and ionization interference matrices have a complex influence on the spatial emission profiles of analyte atoms released in a miniature ICP. The magnitudes of the interference effects are strongly influenced by experimental conditions but can be minimal if proper operating conditions are selected.

ABSTRACT

The magnitude of several classical interelement interferences in a miniature ICP is found to be small but dependent on experimental conditions. The origin and manifestation of these interference (matrix) effects are shown to be complex and influenced most strongly by: 1) observation window in the plasma's tail flame, 2) rf power, and 3) nebulizer gas flow rate. In particular, vaporization interference matrices (Al and PO_4) caused a depression in the intensities of both the neutral atom and ion lines of Ca with the Ca II line experiencing a larger effect than that of Ca I. Conversely, easily ionized elements (such as Na and Cs) enhanced both Ca and Mg neutral atom and ion line intensities, with the atom lines exhibiting a larger increase than those of the ions. Because both the neutral atom and ion lines of Ca and Mg are enhanced by Na and Cs, and to identical degrees, a simple shift in ionization equilibria seems not to produce the observed interference. Clearly, more fundamental knowledge concerning the formation and excitation of atoms in ICP sources is needed before interference mechanisms can be elucidated. However, with the information gained from the present study, compromise conditions for simultaneous multielement analysis can be selected which provide interference levels that are minimal for most, but not all, analyte-matrix combinations and are comparable to those found in conventional ICP sources.

Atomic emission spectrometry (AES) has been revitalized during the past decade through the development of inductively coupled plasma (ICP) excitation sources. The exceptional analytical capabilities of ICP-AES systems have been cited in a recent review (1). However, as with any analytical technique improvements are always possible. Recently, we developed and characterized an ICP which is 33% smaller than conventional ICP sources (2), which can be sustained at low radio-frequency (rf) power levels (i.e., < 1.0 kW) and which requires only 8 L min^{-1} of argon coolant gas; these operational advantages can result in a significant savings for the user in both initial equipment and operating costs. Significantly, a mini-plasma operating under these conditions demonstrated the same analytical capabilities for which conventional ICP sources have become known (i.e., low detection limits, extended linear working curves, high excitation temperatures and simultaneous multielement capabilities).

Another important characteristic of an excitation source is its susceptability to interelement interferences (i.e. matrix effects). It has become increasingly apparent that interferences can be minimized in conventional ICP sources by proper choice of operating conditions, but the origin of such effects is complex and not well understood (3-6). Accordingly, this subject was not treated in our first report (2) so that a more detailed and thorough investigation could be completed. Such an investigation is the subject of the present paper.

The influence of a phosphate matrix on calcium emission is a classical example of a vaporization interference system in flames and has been extensively studied (5,6). The reduced level of this interference and of a similar one (Al on Ca) in the ICP have often been used in the

literature to demonstrate the superiority of the plasma over the flame for analytical applications (9-11). Significantly, Kornblum and de Galan (3) have cited conflicting reports about this interference in the literature. They suggest that changes in analyte emission which have been observed are not solely due to simple changes in the rate of analyte vaporization; rather, a more complex mechanism appears to hold and involves changes in the spatial distribution of analyte free atoms, excitation temperatures and ionization equilibria. Similarly, they have reviewed the ICP literature concerning the influence of easily ionized elements (such as Na and Cs) on analyte emission and have found that these effects are also complex and cannot be explained in terms of simple shifts in ionization equilibria. Most importantly, it has been shown (3,4,12) that the magnitude of all of these interferences depends critically on three primary experimental parameters: 1) observation height in plasma's tail flame, 2) nebulizer gas flow rate and 3) applied rf power.

In the present study, several classical vaporization (PO_4 and Al and Ca) and ionization (Na and Cs on Ca and on Mg) interference systems are investigated in the mini-ICP as a function of the three primary experimental parameters listed above. Detailed spatial emission patterns for both the neutral atom and ion lines of the analyte species are measured in the presence and absence of the interfering matrix. The experiments were designed to provide qualitative information about the nature of interferences in the mini-ICP and to evaluate the probability of establishing useful conditions to minimize their effects. No attempt

was made to use this information to deduce a comprehensive interference mechanism; such a step would require knowledge not yet available about the formation and excitation of atoms in the mini-ICP (3,4,6). In addition, these studies demonstrate that the mini-ICP possesses about the same levels of interference as conventional larger ICP sources.

EXPERIMENTAL

The experimental system employed in this study is the same as previously described (2) except for a slightly modified torch and optical arrangement and a new type of multichannel detection system. The detection system is similar to the ones that Franklin, et al. (13) and Edmonds and Horlick (14) employed to obtain spectral emission profiles of analyte species in flames and plasmas. In addition, several improvements in mini-torch design were incorporated and a cross-flow pneumatic nebulizer utilized for several investigations.

Improved Mini-Torch Design. The basic features of the mini-torch were previously described (2,15); however, several recent modifications have improved torch performance. In one modification, the capillary section at the end of the injection tube (cf., Fig. 2, ref. 2) has been extended the full length of the torch, so the sample injection gas stream is forced to flow in a more laminar pattern. Consequently, the diameter of the injection tube could be increased to 1 mm without affecting plasma stability. The larger-diameter injection tube enables the pneumatic nebulizer to be operated at higher gas flows (where it demonstrates better stability), while low aerosol injection velocities and long sample residence times are maintained (2). Also, polishing the tip of the injection tube avoided problems with clogging and salt build-up.

Other findings also improved mini-plasma performance. To insure plasma stability during low-power operation, the top of the plasma tube (cf., Fig. 2, ref. 2) was positioned 3 mm below the bottom of the load coil. In addition, the tip of the injection tube was cut even with the top of the plasma tube.

Nebulizers. The sample introduction system consists of either a cross-flow (Model TN-1, Plasma-Therm Inc., Kresson, N.J.) or concentric pneumatic nebulizer (2) attached to a dual-tube spray chamber. Ordinarily, the sample solution is delivered to the concentric or cross-flow nebulizers by a peristaltic pump, at a rate of either 0.8 mL min^{-1} or 2.0 mL min^{-1}, respectively. The aerosols generated by these systems are fed directly into the torch (i.e., no desolvation apparatus is employed).

Modified Optical Design. Radiation from the tail flame of the mini-plasma is collected by a spherically concave front-surface mirror (2) and imaged 34.7 cm from the entrance slit of the monochromator. This image is then refocused by a plano-convex lens (f.l. = 7.5 cm, diameter = 2.5 cm, fused silica, Melles Griot, Irvine, CA) onto the monochromator's entrance slit; accordingly, the size of the region observed in the plasma is determined by the entrance slit's dimensions. The center of the plasma source is located 70.5 cm from the mirror's center which is in turn positioned 129.8 cm from the entrance slit of the monochromator. The magnification factor of the total system is 0.625. An iris is placed at the lens to act as an aperture stop.

To reduce astigmatism, all off-axis angles have been minimized in this optical arrangement. The optical components are positioned so a point 20 mm above the load coil (the center of the desired observation zone) and the centers of the mirror and entrance slit are all in the same horizontal plane. Importantly, the geometry of the optics is such that the sagittal image (produced by the small angle between the mirror normal and the center of the observation zone in the horizontal plane) is the object for the lens; therefore, submillimeter spatial resolution in the vertical plane is achievable (16-18).

Detection System. The detection system consists of a silicon intensifier target vidicon tube (SIT) and an optical multichannel analyzer (Model 1205D Intensifier Detector Head, Model 1205A OMA Console, Princeton Applied Research, Princeton, N.J.). The signal is displayed on either a CRT monitor (Model 603, Tektronix, Beaverton, OR) or an X-Y recorder (Model 2000 Omnigraphic, Houston Instruments, Bellaire, TX). The target of the SIT is 2.5 mm wide and 12.5 mm high and is divided into 500 channels on 25-μm centers; each channel is 25 μm wide. Because the target is oriented vertically in the exit focal plane of the monochromator, it acts as a 2.5-mm wide by 12.5-mm high exit slit. The stigmatic monochromator then provides an assessment of emission intensity as a function of height in the plasma. Moreover, the 500 channels in the SIT enable a very high resolution spatial picture to be obtained. Because practical analyses usually employ emission intensities which are integrated over the depth of the source, no effort was made here to radially resolve the emission signals from the mini-ICP (i.e., no Abel inversion is applied).

Signals from all 500 channels of the SIT are sent to the console of the optical multichannel analyzer for processing. During every read-in cycle (32 ms accumulation cycle interval), the light signal integrated since the last scan at each of the 500 target elements is digitized and added to the contents of a predefined memory. The number of input cycles scanned into memory is selected by the operator. Two memories are provided, enabling background subtraction to be performed. In all curves reported or displayed in this report, this background subtraction has been carried out.

Geometrically, the optics and detector are aligned so the target views a vertical slice located in the middle of the plasma's tail flame and centered 20 mm above the load coil. Because the height of the entrance slit is made equal to that of the SIT target (i.e., 12.5 mm), the detector observes a track starting at 10 mm and extending to 30 mm above the load coil.

The uniformity of the spatial response of the optics and detection system was evaluated by placing a spatially homogeneous light source where the plasma's tail flame is normally located. Ideally, a plot of intensity versus height in the plasma (i.e., channel number) should then be flat; in reality, the system demonstrated a fairly flat response but with a slight deterioration in signal near the edges of the target (i.e., ~20% for the first and last 50 channels). The origin of this inhomogeneous response was determined to be in the SIT itself; this non-linear response could be corrected by appropriate signal processing techniques but no correction was applied in this study. In addition, the unusually large deviations observable in all the emission profiles at 15 mm above the load coil (cf., for example, Fig. 5) and the flat response observed

in some plots at 10 to 12 mm (cf. Figure 7A) are also due to imperfections in the SIT and do not represent true spatial structure in the plasma.

Another important feature of the dispersion and detection system is its spectral bandpass. Even though the monochromator provides a high linear dispersion, the large target size of the SIT (2.5 mm) establishes the system bandpass at 9.75 Å. Consequently, in all the studies reported below, spectral interferences were carefully evaluated and proven to be inconsequential.

Operating Conditions for Spatially Profiling the Mini-ICP. After a nebulizer is selected, the mini-plasma is ignited under the operating conditions listed in Table I. A concentric nebulizer was employed for the vaporization interference studies and a cross-flow for the ionization interference investigations. The cross-flow nebulizer produces a larger quantity of aerosol than the concentric for a given gas flow rate; accordingly, an approximately one-order-of-magnitude increase in signal is realized. However, the larger quantities of aerosol also cause plasma instability at low rf powers. Therefore, when this type of nebulizer is employed, different gas flows and higher rf power levels are required (cf., Table I).

The iris and entrance slit width are next adjusted so the intensity of the light striking the SIT does not saturate it. Because this study is concerned only about vertical spatial resolution, a change in entrance slit width has as its principal effect an adjustment in the intensity of the dispersed radiation which strikes the detector. Significantly, the highest line-to-background ratios are achieved at the smallest (but greater than the diffraction limit) possible slit widths.

Once operating conditions are established, analyte (or analyte plus interfering matrix) is introduced and the resulting signal is read from the SIT into console memory A. A blank solution (distilled-deionized H_2O or a matrix-matched blank) is then aspirated and the corresponding signal read into memory B. Memory B is subtracted from A channel-by-channel and the resulting background-corrected signal is plotted on the X-Y recorder. Plots of this nature are generated as a function of rf power and nebulizer gas flow to obtain a complete profile of the interferent's influence on analyte emission intensity.

Reagents. Stock solutions were prepared as suggested by Dean and Rains (19), using reagent grade salts and acids as required. The Na and Cs concomitants were added as solutions of reagent grade chlorides. Phosphorus was added as reagent grade $(NH_4)_2HPO_4$ in the Ca-PO_4 system, whereas the Al concomitant solutions were prepared from the metal. Ten percent (by volume) of concentrated HCl was added to all solutions so that any acid effects would not bias the measurements.

RESULTS AND DISCUSSION

Effects of rf Power and Nebulizer Flow Rate on Ca Emission Profiles. A spatial profile of Ca neutral atom emission (422.7 nm) is shown in Figure 1. These plots were obtained when a 50 $\mu g\ mL^{-1}$ Ca solution was introduced by a concentric nebulizer into the mini-ICP operating under the conditions cited in Table I. The five curves in each section of the figure correspond to five different nebulizer gas flow rates. The three frames in the figure (labelled X, Y and Z) correspond to different

rf power levels (750 W, 1.0 kW and 1.25 kW, respectively) established for the measurements. The relative intensity scales on the three frames are not the same.

A number of important trends are evident in the profiles of Figure 1. Within any one frame (i.e., at any particular rf power setting), an increase in nebulizer gas flow produces a higher intensity of analyte emission and causes the point of maximum intensity to shift higher in the plasma's tail flame. Consequently, the optimal nebulizer gas flow will be different from region to region in the plasma. For example (see Figure 1, frame Y), if a 2-mm-high observation window were centered 15 mm above the load coil, a nebulizer flow of 1.19 L min^{-1} would provide the highest emission signal. However, if the window were centered at 20 mm, a 1.30 L min^{-1} flow rate would be optimal. These changes in analyte emission characteristics result from the fact that both aerosol formation and transport properties and sample injection velocities (and residence times) are both affected by changes in nebulizer gas flow rate.

Another interesting feature in Figure 1 is the remarkable influence that rf power exerts on the position of peak analyte emission. For example, curve 5 peaks in intensity lower in the plasma as the power is increased from 750 W (frame X) to 1.25 kW (frame Z). Importantly, the relative intensity scales decrease in sensitivity from frame X to Z, indicating that Ca I emission intensity increases with rf power.

Figure 2 contains a set of emission profiles similar to those in Figure 1 but for the calcium ion line at 393.4 nm. The intensity of the Ca II emission is much stronger than the Ca I line discussed above.

Clearly, the spatial behavior of Ca II (Figure 2) is quite different from that of Ca I (Figure 1).

In frame X (750 W) of Figure 2, the emission is greatest at a nebulizer flow rate of 0.86 L min^{-1} (curve 1); at a slightly higher flow rate (curve 2) the intensity drops sharply, but remains relatively constant as the flow is increased further (curves 3 to 5). The peak in emission intensity also shifts higher in the plasma as the nebulizer flow is increased. Spatial shifts in peak intensity also occur as a function of nebulizer flow rate in frames Y and Z, but to a lesser extent. Not surprisingly, when the rf power applied to the mini-plasma is increased, maximum emission intensities are achieved at higher nebulizer gas flow rates (e.g., curve 2 demonstrates the highest analyte emission at 1.0 kW whereas curve 3 yields the maximum at 1.25 kW). Figure 2 also shows that the point of maximum emission shifts lower in the plasma as rf power is increased (compare curve 1 in frames X, Y and Z). Although not obvious from Figure 2 because of different scale factors in the various curves, Ca II emission intensity also increases with rf power.

Figures 1 and 2 demonstrate that Ca II emission intensity changes more with operating conditions than does that of Ca I, but spatial shifts in the emission profiles are smaller for Ca II than Ca I. Edmonds and Horlick (14) observed spatial emission profiles similar to those described above for neutral atom and ion lines of calcium, but in a conventional ICP. This similarity suggests that the excitation behavior and capabilities of the two sources are comparable.

Spatial Profiles for Classical Solute Vaporization Interference Systems. In this section the influence of an Al or phosphate matrix on the spatial emission profiles for Ca neutral atom and ion species is

examined. Also, the influence of varying rf power and nebulizer gas flow on these interference effects is investigated. Clearly, to present curves such as those in Figures 1 and 2 for all these combinations would be confusing and redundant. Accordingly, only one interference system (the effect of Al on Ca I) will be presented in detail; for all other combinations, just one spatial profile will be reproduced to indicate the magnitude of the effect. All other influences will then be summarized by comparison with the displayed profile. In all the Al and PO_4 interference studies, the added matrix does not change the background level; therefore, the blank used in these studies was distilled-deionized H_2O.

Figure 3 illustrates the influence of an Al matrix on the Ca I (422.7 nm) spatial emission profile as a function of rf power. The signals in frames X, Y and Z are obtained at powers of 750 W, 1.0 kW and 1.25 kW, respectively. Curve A in each frame was obtained during the aspiration of a 50 $\mu g\ mL^{-1}$ Ca solution while curve B results when the Ca solution contains Al at a molar ratio of 50 to 1 (Al:Ca).

At low rf power (frame X), the Ca I emission intensity is substantially depressed when aluminum is present. However, at higher powers (frames Y and Z) either an enhancement or a depression might be measured, depending on the portion of the plasma's tail flame which is observed. For example, if the spectroscopic observation window in frame Y extended from 10 to 15 mm above the load coil, a depression would be measured. In contrast, a viewing window from 15 to 20 mm would register an enhancement. Significantly, if a window covering the entire region from 10 to 20 mm were employed, the changes would nullify

each other and no interference would be indicated. Clearly, this latter option would be selected for routine analytical measurements. In each frame of Figure 3 the occlusion of Ca in an aluminum matrix causes the emission profile to shift higher in the plasma and to spread out over a larger vertical region. This shift in peak intensity is most evident at low rf power (frame X).

Figure 4 shows the effects of added Al and varying nebulizer gas flow on the spatial profile of Ca I; the rf power is fixed at 1.0 kW. Frames 1 through 5 are plotted at nebulizer flow rates (L min^{-1}) of 0.86, 0.97, 1.08, 1.19 and 1.30, respectively. As in Figure 3, a slight depression is observed low in the plasma and enhancement high in the plasma. Significantly, the magnitude of the interference rises and the spatial shifts in the emission profile become larger (compare frame 2 and 5) as the nebulizer flow is increased.

The plots in Figures 3 and 4 demonstrate that interferences can be minimal in the mini-ICP if proper operating conditions are selected. Conversely, the degree and polarity of an interference is strongly influenced by the exact experimental parameters employed.

The Ca II (393.4 nm) spatial emission profile plotted in Figure 5 was obtained under the same operating conditions as frame 2 of Figure 4 (for Ca I) and shows a slightly greater depression when Al is added than was observed for Ca I. In addition, the shape and position of the Ca II emission profile (Figure 5) does not change as much when the Al matrix is present as did those of Ca I; accordingly, an Al-caused signal depression is measured for Ca II no matter what portion of the plasma's tail flame is observed. Changes in rf power and nebulizer gas flow do not influence these interference effects greatly,

although a small reduction in the degree of interference occurs as higher rf powers and lower nebulizer gas flows are employed.

Spatial emission profiles for Ca I and Ca II in the presence and absence of a phosphate matrix (PO_4:Ca molar ratio 50:1) are illustrated in Figure 6. Figures 4 (frame 2) and 5 were obtained under the same operating conditions as Figures 6A and 6B. A comparison of these four plots reveals that a similar depression in Ca I and Ca II emission intensity occurs regardless of whether the matrix is Al or phosphate but the magnitude of the interference is less with PO_4. In fact, when a complete series of emission profiles for Ca I and Ca II is examined (similar to Figures 3 and 4), the same spatial shifts and changes with operating conditions are found for phosphate as previously described for Al. The only difference is a slight, but surprising, increase in the magnitude of the Ca- phosphate interference as rf power is increased.

Effect of Easily Ionized Species (Na and Cs) on Ca and Mg Emission Profiles. In Figure 7, the influence of a Na matrix on the spatial emission profiles of Ca neutral atom and ion lines is illustrated. A slight increase (~2%) in the background level occurs when only the interference matrix is aspirated, particularly at the Ca I line; however, in both cases distilled-deionized H_2O is used as blank.

Overall, there is a large enhancement in the Ca I line intensity when a Na matrix is present (cf., Figure 7A). Interestingly, the magnitude of the interference peaks at 1.0 kW and 1.08 L min^{-1} and declines as either rf power or nebulizer flow is changed. Also, the maximum in the Ca I emission intensity profile shifts slightly lower in the plasma when the Na matrix is present. However, like the influence

From Figure 8B it can be seen that the Ca II emission can be either enhanced or depressed by a Cs matrix depending on the exact point of observation; however, the level of interference is much smaller for Ca II than Ca I and is absent if an "averaging" window between 15 and 18 mm is selected. The spatial position of the Ca II emission profile is shifted lower in the plasma by the Cs matrix and the amount of the shift grows as the nebulizer gas flow increases. Importantly, the interference becomes negligible at high rf powers (i.e., 1.0 kW or greater) and low nebulizer gas flows.

The effects of Na and Cs on the emission profiles of Mg neutral atom (285.2 nm) and ion (279.5 nm) lines are almost identical to those for Ca and are therefore not reproduced here. For both matrices the Mg II line is less affected than Mg I emission and the same spatial shifts that were observed in the Ca emission patterns occur. An enhancement in the Mg lines is caused by both Na and Cs but the magnitude of the effect can be minimized through judicious selection of operating parameters. These matrices caused a noticeable enhancement in the background emission level at the Mg lines; therefore, the sample and blank solutions were matrix-matched.

Interference Effects Under Compromise Conditions for Simultaneous Multielement Analysis. One of the most-cited advantages of ICP sources is their ability to perform simultaneous multielement analysis. Accordingly, compromise experimental conditions must be available which provide high sensitivities and minimal matrix effects for a large number of elements. The present study reveals that operating conditions (i.e., observation height, rf power and nebulizer gas flow rate) can have a considerable

of Al and phosphate on Ca II, the effect of Na on the position of the Ca I emission profile does not change with operating conditions.

Figure 7B shows that Ca II emission is slightly enhanced in the presence of a Na matrix, but far less so than for Ca I. However, the Ca II emission profile tends to shift lower in the plasma when the Na matrix is present. Unlike for the neutral atom line, the amount of this shift changes with operating conditions; at higher nebulizer flows or lower rf powers, a larger shift occurs. Accordingly, either enhancements or depressions in Ca II signal intensity might be seen when Na is added, depending on the exact size of the observation window and its position in the plasma's tail flame. This same sort of response is observed for Ca I in the presence of phosphate or Al. Significantly, the amount of interference decreases as rf power is increased and nebulizer gas flow is reduced; it is negligible if proper operating conditions are selected.

The effects of a Cs matrix on the Ca neutral atom and ion lines are shown in Figure 8. No changes in background emission occur when a Cs matrix is introduced and distilled-deionized H_2O can therefore be employed as the blank. By comparing Figures 7A and 7B with 8A and 8B, one observes that Cs has about the same effect as Na on the spatial emission profiles of Ca I and Ca II.

As with Na, the Cs matrix significantly enhances the emission intensity of the Ca I line and shifts the profile slightly lower in the plasma. The magnitude of the shift does not change greatly with operating conditions although the amount of interference is reduced by increasing rf power and decreasing nebulizer gas flow.

influence on the magnitude of the matrix effects exhibited by the mini-ICP. Significantly, the information gained from this study reveals that conditions can be selected so that interferences are minimal in most cases.

One important experimental condition is the size and position of the spectrometer's observation window. A tall viewing window (i.e., 10 mm) centered at 15 mm above the load coil will provide two advantages: 1) the system will be less sensitive to spatial shifts in emission profiles (i.e., enhancements and depressions as shown in Figure 8B will tend to offset each other) and 2) the measured signal will be increased, providing improved signal-to-background (and presumably S/N) ratios (i.e., low detection limits). In most cases, the small but finite interferences are diminished by operating the mini-ICP at high rf power levels; Figures 3 through 8 show that 1.0 kW is adequate.

The third experimental parameter is nebulizer gas flow rate. Throughout these studies, the lowest interference levels were measured at the lowest nebulizer flow rates. However, pneumatic nebulizers become unstable at low gas flows. Accordingly, the following compromise conditions are suggested for routine work: 0.97 L min^{-1} for the concentric nebulizer used in the phosphate and Al studies and 0.86 L min^{-1} for the cross-flow nebulizer used in the Na and Cs investigations.

Table II lists the matrix effects exhibited by a mini-ICP operating under these compromise conditions. The matrix effect is expressed as the percentage difference in the net line signal (sample minus blank signal) of an analyte solution by itself and with the interferent matrix added. Overall, the interferences are quite small except for the influence of easily ionized species on the neutral atom lines of Ca and

Mg. Significantly, the magnitudes of the interferences are comparable to those exhibited by conventional ICP systems

CONCLUSIONS

Experimental conditions (i.e., observation height in the plasma's tail flame, applied rf power, and nebulizer type and gas flow rate) can significantly influence analyte spatial emission characteristics in a mini-ICP. In addition, the occlusion of the analyte in several classical interference matrices (vaporization and ionization type) was also found to alter the analyte's spatial emission profile. The magnitude of the interferent's effect was highly influenced by experimental conditions.

Classical vaporization interference systems (such as Al and phosphate) caused a depression in both the ion and neutral atom lines of calcium in the mini-ICP; however, the Ca II line exhibited a larger effect than did Ca I. Significantly, in both cases (Al and phosphate) the emission profiles of the neutral atom line were shifted higher in the plasma when the matrix was present. Possibly, the analyte atoms are being trapped in a refractory matrix (4) which would require longer residence times in order to be efficiently atomized. The fact that this shift is minimized at high rf powers and low nebulizer gas flows also supports a vaporization interference mechanism. Interestingly, these shifts were not observed for the Ca II line, indicating that other excitation mechanisms prevail for this species. Even though Horlick, et al. (14) did not see identical results in a conventional plasma, they did detect these same shifting patterns.

Ionization interferences can be significant and, in contrast to the vaporization interferences, have a stronger influence on neutral atom

lines than on ion lines. The spatial emission profiles of both the ion and neutral atom lines of Mg and Ca were shifted lower in the plasma when either a Na or Cs matrix was introduced. A change in the mini-plasma's excitation temperature profile upon adding these matrices could have caused this shift. Changes in excitation temperature such as this have been reported by Kornblum and de Galan (3) in conventional ICP sources. Moreover, the fact that both the neutral atom and ion lines of the analyte species were enhanced by Cs and Na and to identical degrees does not support a mechanism based on a simple change in ionization equilibria. Clearly, more fundamental knowledge is needed concerning the effect of sample matrix on solute volatilization, plasma temperatures and ionization equilibria before interference mechanisms can be elucidated in the mini-ICP. These studies are currently underway in this laboratory.

LITERATURE CITED

(1) Barnes, R. M. CRC Crit. Rev. Anal. Chem. 1978, 7, 303.

(2) Savage, R. N.; Hieftje, G. M. Anal. Chem. 1979, 51, 408.

(3) Kornblum, G. R.; deGalan, L. Spectrochim. Acta, Part B., 1977, 32, 455.

(4) Larson, G. F.; Fassel, V. A.; Scott, R. H.; Kniseley, R. N. Anal. Chem. 1975, 47, 238.

(5) Mermet, J. M.: Robin, J. P. Anal. Chim. Acta, 1975, 70, 271.

(6) Boumans, P. W. J. M.; deBoer, F. J. Spectrochim. Acta, Part B, 1976, 31, 355.

(7) Alkamade, C. Th. J.; Herrmann, R. "Fundamentals of Analytical Flame Spectroscopy," Halsted Press: New York, 1979.

(8) Alkemade, C. Th. J. Anal. Chem. 1966, 38, 1252.

(9) Greenfield, S.; Jones, I. Ll.; Berry, C. T. Analyst, 1964, 89, 713.

(10) Dickinson, G.W.; Fassel, V.A. Anal. Chem. 1969, 41, 1021.

(11) Fassel, V.A.; Kniseley, R. N. Anal. Chem. 1974, 46, 1155A.

(12) Boumans, P. W. J. M.; deBoer, F. J. Spectrochim. Acta, Part B, 1975, 30, 309.

(13) Franklin, M. L.; Baber, C.; Koirtyohann, S. R. Spectrochim. Acta, Part B, 1976, 31, 589.

(14) Edmonds, T. E.; Horlick, G. Appl. Spectrosc. 1977, 31, 536.

(15) Sexton, E.; Savage, R. N.; Hieftje, G. M. accepted for publication in Appl. Spectrosc.

(16) Goldstein, S. A.; Walters, J. P. Spectrochim. Acta, Part B, 1976, 31, 201.

(17) Goldstein, S. A.; Walters, J. P. Spectrochim. Acta, Part B, 1976, 31, 295.

(18) Salmon, S. G.; Holcombe, J. A. Anal. Chem. 1978, 50, 1714.

(19) Dean, J. A.; Rains, T. C. "Flame Emission and Atomic Absorption Spectrometry," Vol. 2; Marcel Dekker: New York, 1971; Chapter 13.

ACKNOWLEDGMENT

The authors are indepted to Ralph Lemke for writing several of the computer programs used for data analysis.

CREDIT

Supported in part by the Office of Naval Research and by the National Science Foundation through grants CHE 76-10896 and CHE 77-22152.

TABLE I GENERAL OPERATING CONDITIONS FOR MINI-ICP SYSTEM

	concentric nebulizer	cross-flow nebulizer
rf power[a], W	750-1250[b]	850-1250[b]
Argon flows, L min^{-1}		
coolant	7.9	8.3
plasma	0.3	0
nebulizer	0.86-1.30[b]	0.75-1.08[b]

[a] Forward power output from the rf generator.

[b] Range of operating conditions studied.

TABLE II INTERFERENCES EXHIBITED BY MINI-ICP UNDER COMPROMISE CONDITIONS

Analyte (wavelength) \ Interferent	% Change in analyte signal when interferent added[a]			
	Al	PO_4	Na	Cs
Ca I (422.7 nm)	-4	+4	+39	+26
Ca II (393.4 nm)	-14	-5	+6	+2
Mg I (285.2 nm)			+40	+42
Mg II (279.5 nm)			+10	+23

[a] + denotes enhancement and - depression of analyte signal. No table entry indicates that combination was not studied.

FIGURE CAPTIONS

Figure 1 Spatial emission profiles of Ca I (422.7 nm) as a function of rf power (Frame X - 750 W; Y - 1.0 kW; Z - 1.25 kW) and nebulizer flow rate (Curve 1 - 0.86 L min^{-1}; 2 - 0.97 L min^{-1}; 3 - 1.08 L min^{-1}; 4 - 1.19 L min^{-1}; 5 - 130 L min^{-1}). A concentric nebulizer introduced a 50 µg mL^{-1} Ca solution into the plasma. Entrance slit width = 30 µm. Intensity scales are not equal in X, Y and Z. See text for discussion.

Figure 2 Spatial emission profiles of Ca II (393.4 nm) as a function of power and nebulizer gas flow (same format as Figure 1). A concentric nebulizer introduced a 50 µg mL^{-1} solution. Entrance slit width = 20 µm. Intensity scales are not equal in frames X, Y, and Z. See text for discussion.

Figure 3 Effect of Al on Ca I (422.7 nm) emission profiles with changing rf power levels (Frame X - 750 W; Y - 1.0 kW; Z - 1.25 kW). Curve A represents analyte (50 µg/mL^{-1} Ca) signal and curve B analyte plus interferent (50:1 molar ratio Al:Ca). Concentric nebulizer operated at 1.08 L min^{-1}. Entrance slit width = 30 µm. Intensity scales are not equal in frames X, Y, and Z.

Figure 4 Effect of Al on Ca I (422.7 nm) emission profiles as a function of changing nebulizer (concentric) gas flow rate (Frame 1 -

0.86 L min^{-1}; 2 - 0.97 L min^{-1}; 3 - 1.08 L min^{-1}; 4 - 1.19 L min^{-1}; 5 - 1.30 L min^{-1}). Curve A represents analyte (50 µg mL^{-1} Ca) signal and curve B analyte plus interferent (50:1 molar ratio Al:Ca). Radiofrequency power applied = 1.0 kW. Entrance slit width = 30 µm. Intensity scales are not equal in frames 1-5.

Figure 5 Effect of Al on Ca II (393.4 nm) emission profile. A concentric nebulizer (operating at 0.97 L min^{-1}) introduced a 50 µg mL^{-1} Ca solution (Curve A) and the same solution with aluminum added (Curve B) in a molar ratio of 50:1 (Al:Ca). Entrance slit width = 20 µm and rf power applied = 1.0 kW.

Figure 6 Effect of phosphate on Ca I (422.7 nm) and Ca II (393.4 nm) spatial emission profiles. The intensity scales in Figures 6A and 6B are not equal. A concentric nebulizer (operating at 0.97 L min^{-1}) introduced a 50 µg mL^{-1} Ca solution (Curve A) and the same solution with aluminum added (Curve B) in a molar ratio of 50 to 1 (Al:Ca). Rf power applied = 1.0 kW.

A) Ca I response (top plot): Entrance slit width = 30 µm.

B) Ca II response (bottom plot): Entrance slit width = 20 µm.

Figure 7 Effect of Na on Ca I (422.7 nm) and Ca II (393.4 nm) spatial emission profiles. The intensity scales in Figures 7A and 7B are not equal. A cross-flow nebulizer (operating at 0.86 L min^{-1}) introduced a 5 µg mL^{-1} Ca solution (Curve A) and the same solution with sodium added (Curve B) in a molar ratio of 140 to 1 (Na:Ca). Rf power applied = 1.0 kW.

A) Ca I response (top plot): Entrance slit width = 30 µm.

B) Ca II response (bottom plot): Entrance slit width = 20 µm.

Figure 8 Effect of Cs on Ca I (422.7 nm) and Ca II (393.4 nm) spatial emission profiles. The intensity scales in Figures 8A and 8B are not equal. A cross-flow nebulizer (operating at 0.86 L min^{-1} Ca solution (Curve A) and the same solution with cesium added (Curve B) in a molar ratio of 140 to 1 (Cs:Ca). Rf power applied = 1.0 kW.

A) Ca I response (top plot): Entrance slit width = 30 µm.

B) Ca II response (bottom plot): Entrance slit width = 20 µm.

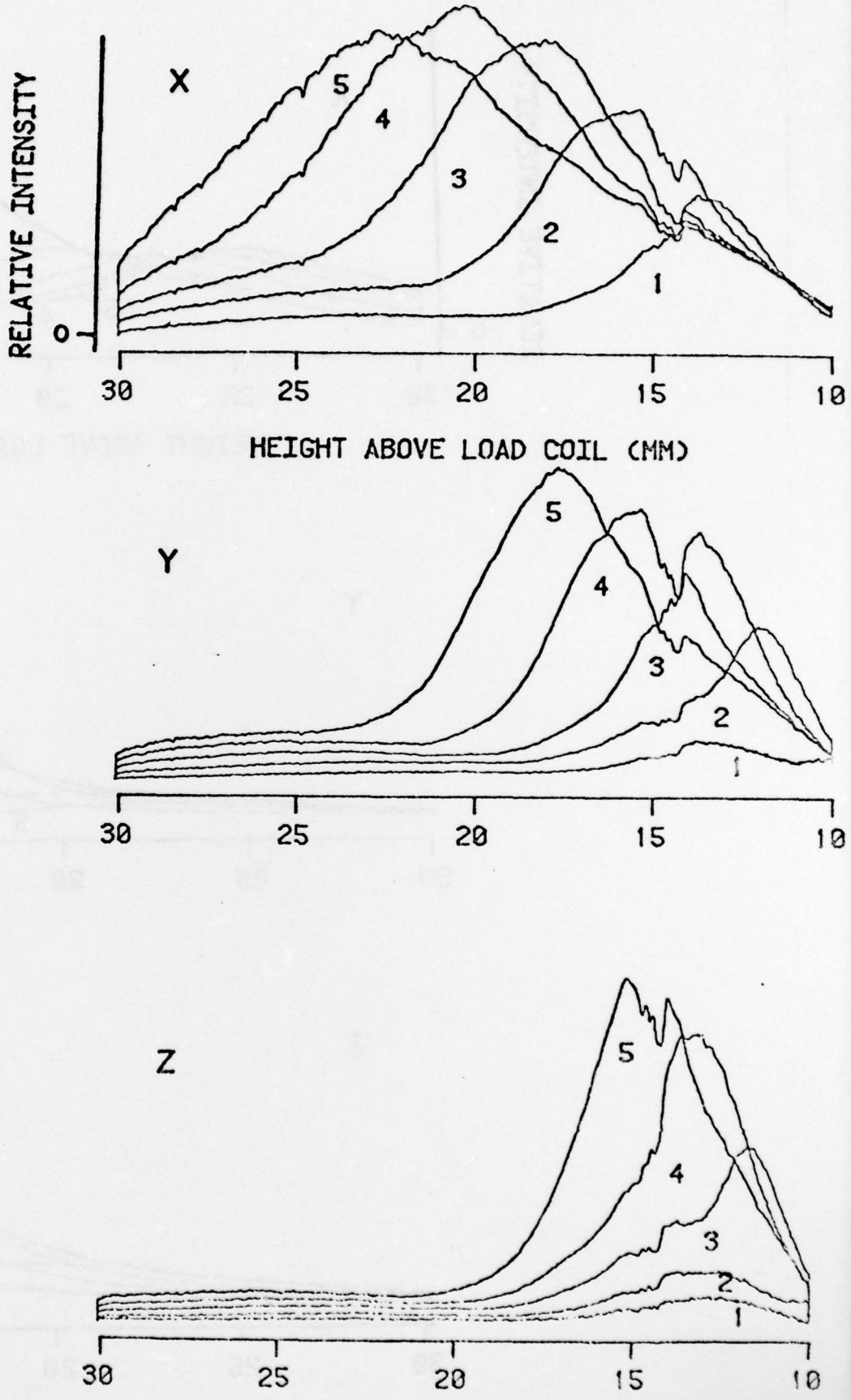
RELATIVE INTENSITY
0
X
5
4
3
2
1
30
25
20
15
10
HEIGHT ABOVE LOAD COIL (MM)
Y
5
4
3
2
1
30
25
20
15
10
Z
5
4
3
2
1
30
25
20
15
10

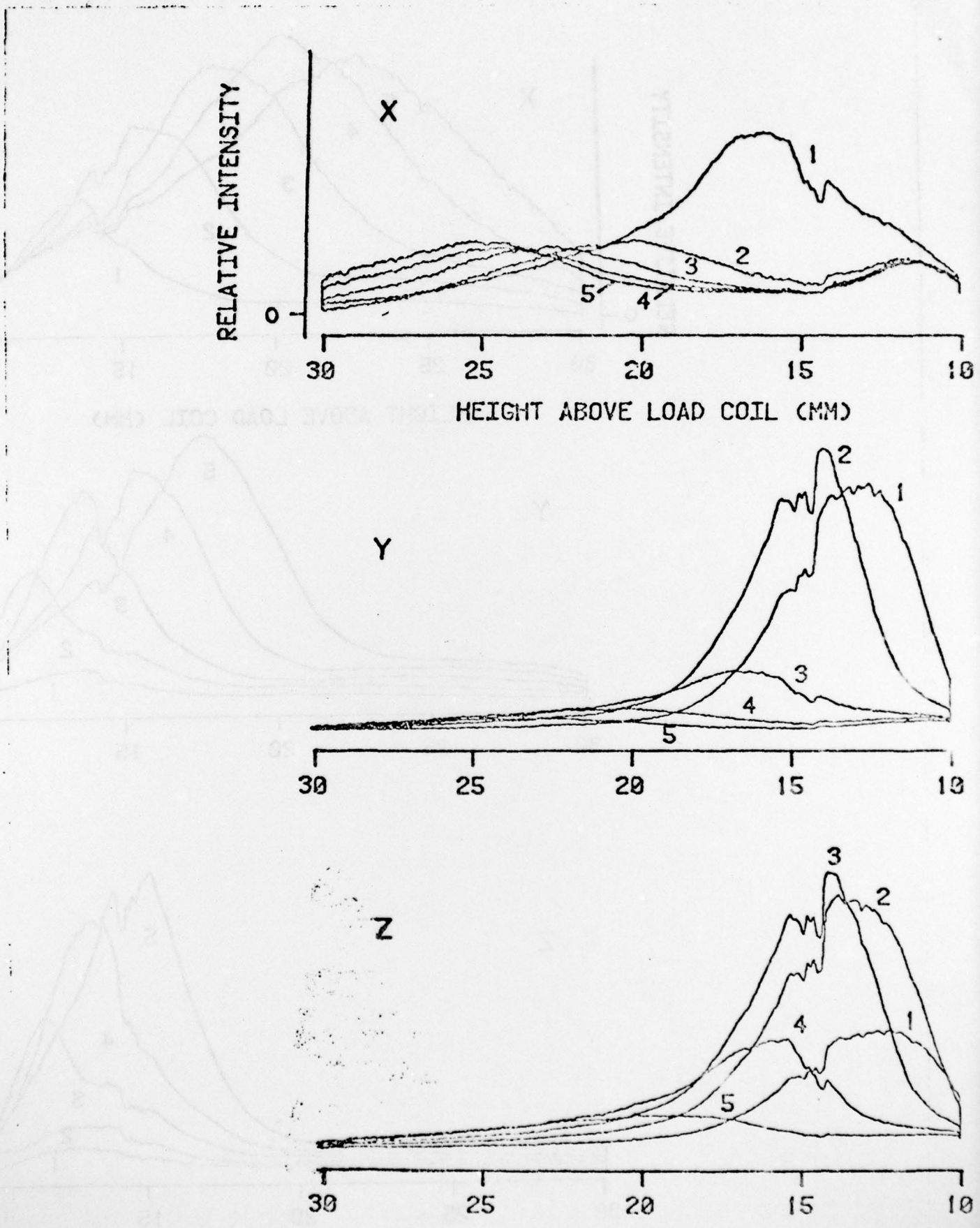
RELATIVE INTENSITY
X
1
2
3
5
4
0
30
25
20
15
10
HEIGHT ABOVE LOAD COIL (MM)
Y
2
1
3
4
5
30
25
20
15
10
Z
3
2
4
1
5
30
25
20
15
10

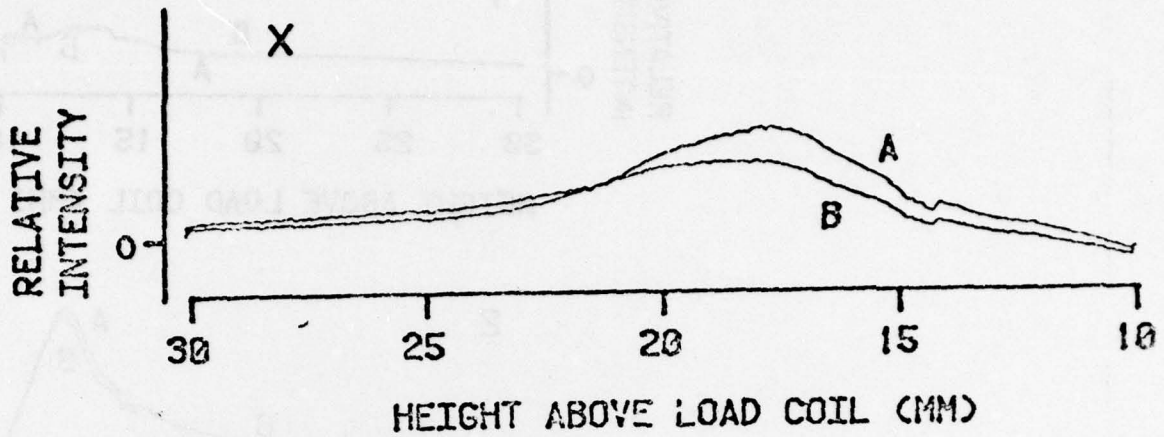
X
RELATIVE INTENSITY
0
A
B
30
25
20
15
10
HEIGHT ABOVE LOAD COIL (MM)

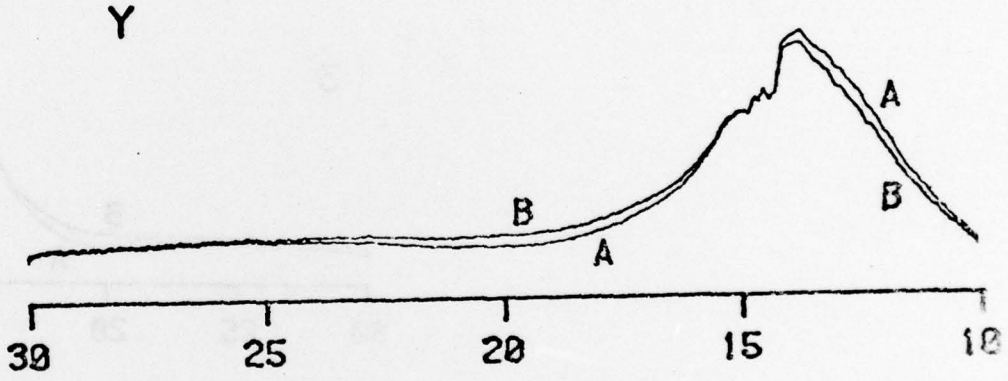
Y
A
B
B
A
30
25
20
15
10

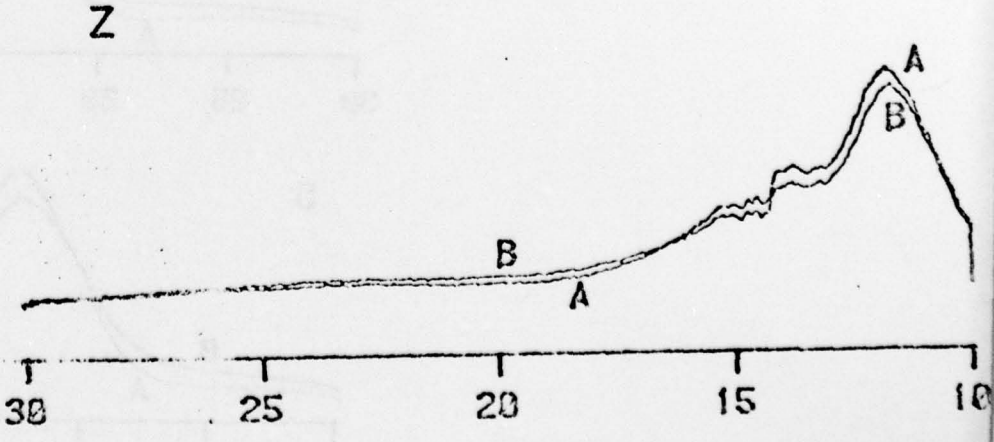
Z
A
B
B
A
30
25
20
15
10

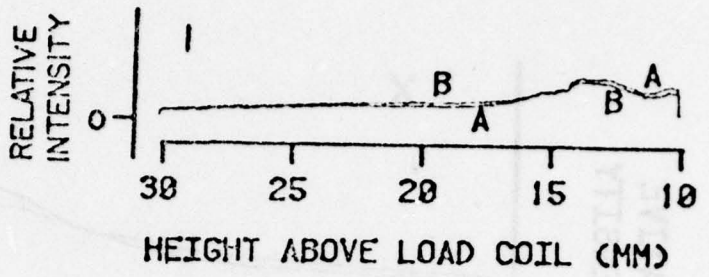
RELATIVE INTENSITY
0
1
B
A
B
A
30
25
20
15
10
HEIGHT ABOVE LOAD COIL (MM)

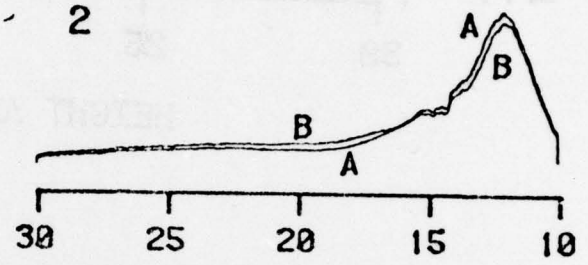
2
A
B
B
A
30
25
20
15
10

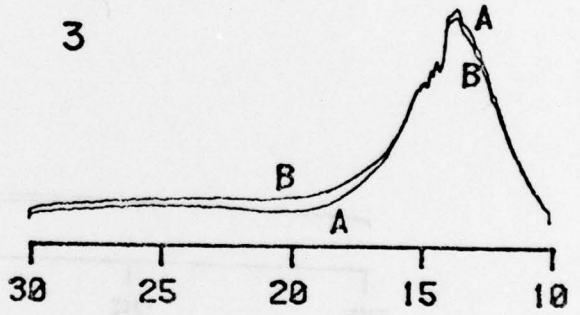
3
A
B
B
A
30
25
20
15
10

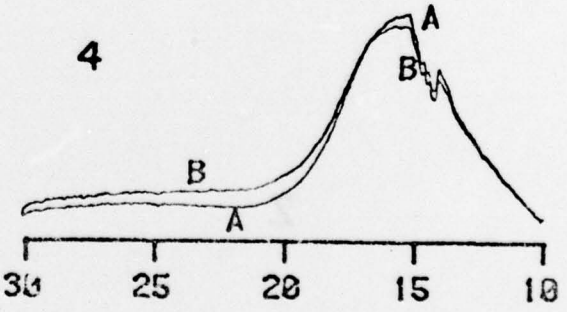
4
A
B
B
A
30
25
20
15
10

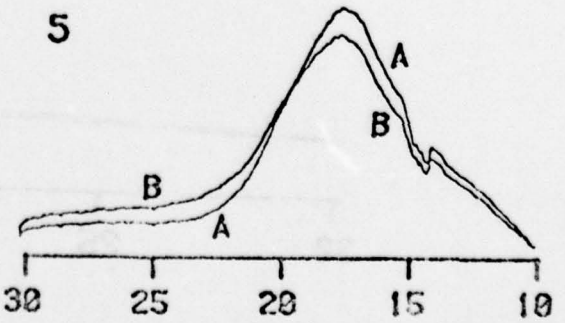
5
A
B
B
A
30
25
20
15
10

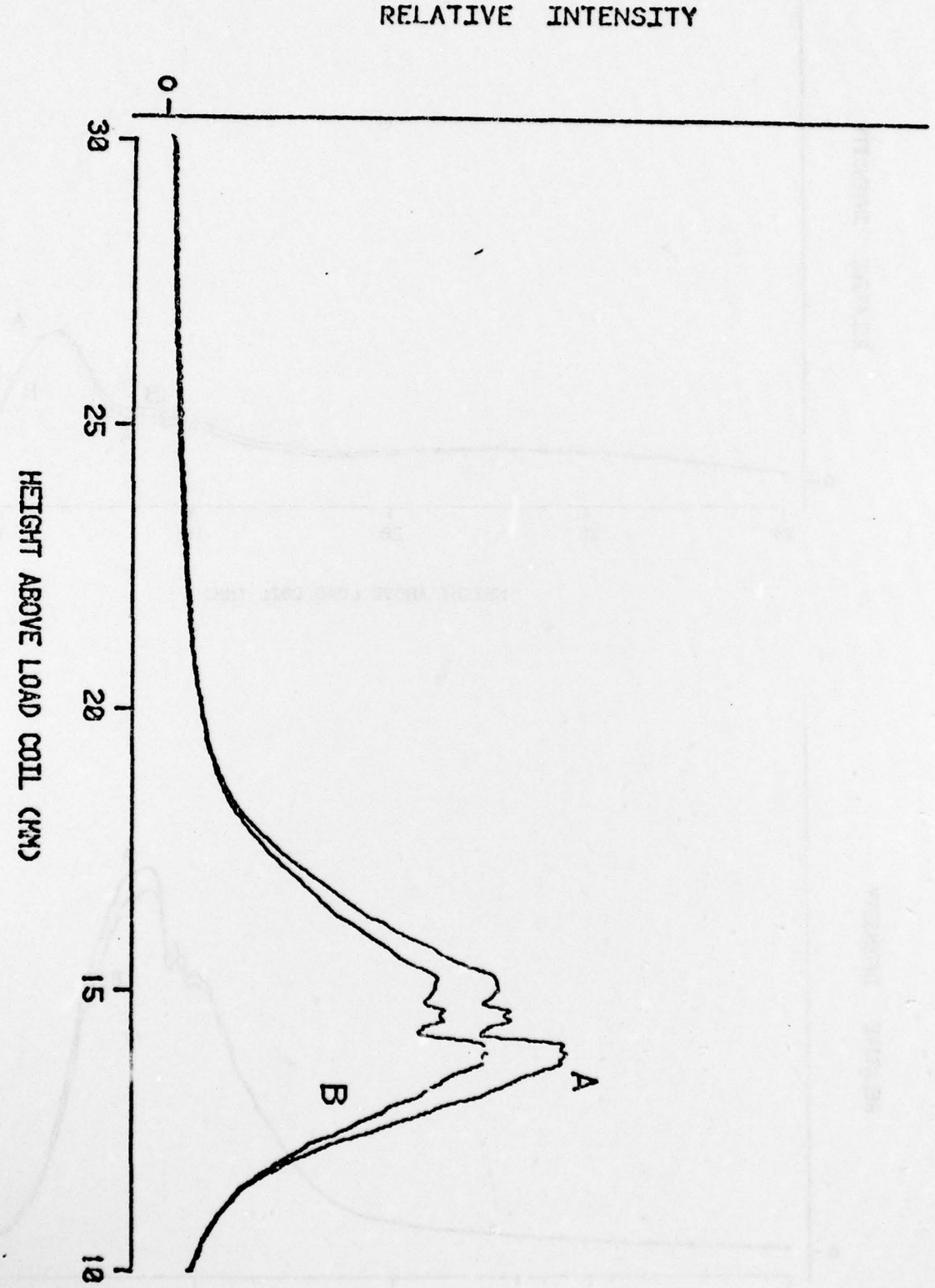
RELATIVE INTENSITY
0
30
25
20
15
10
HEIGHT ABOVE LOAD COIL (KM)
A
B

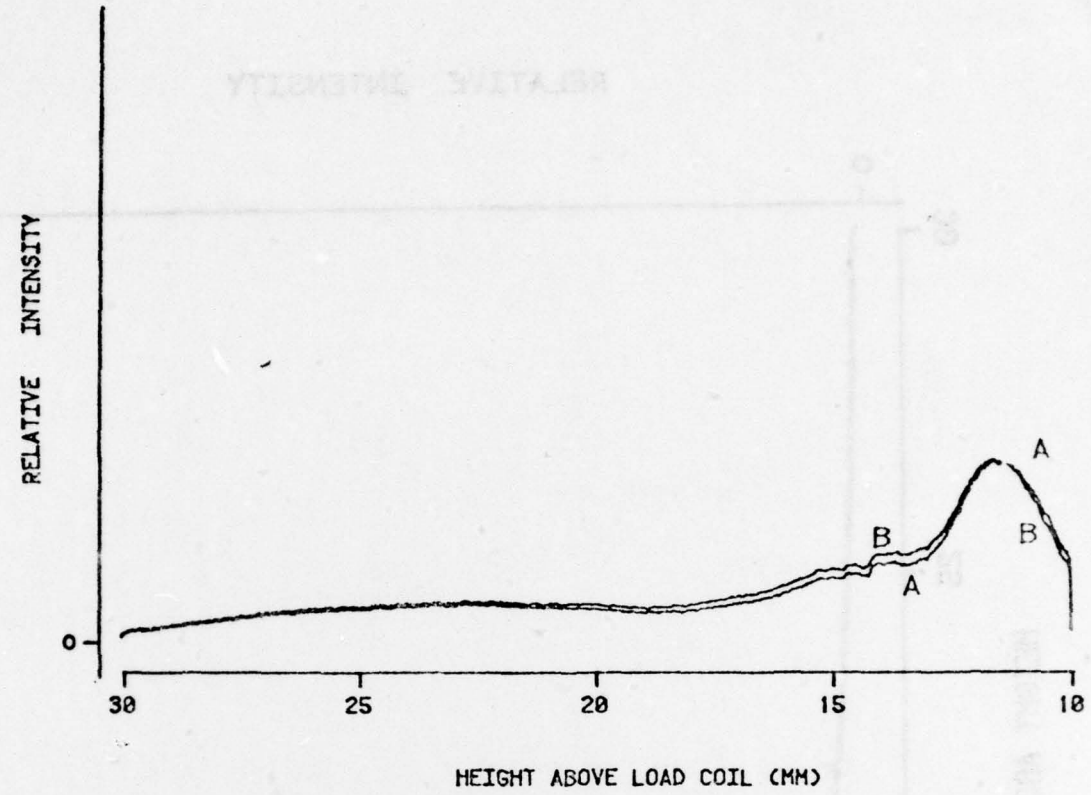
RELATIVE INTENSITY
0
A
B
B
A
30
25
20
15
10
HEIGHT ABOVE LOAD COIL (MM)

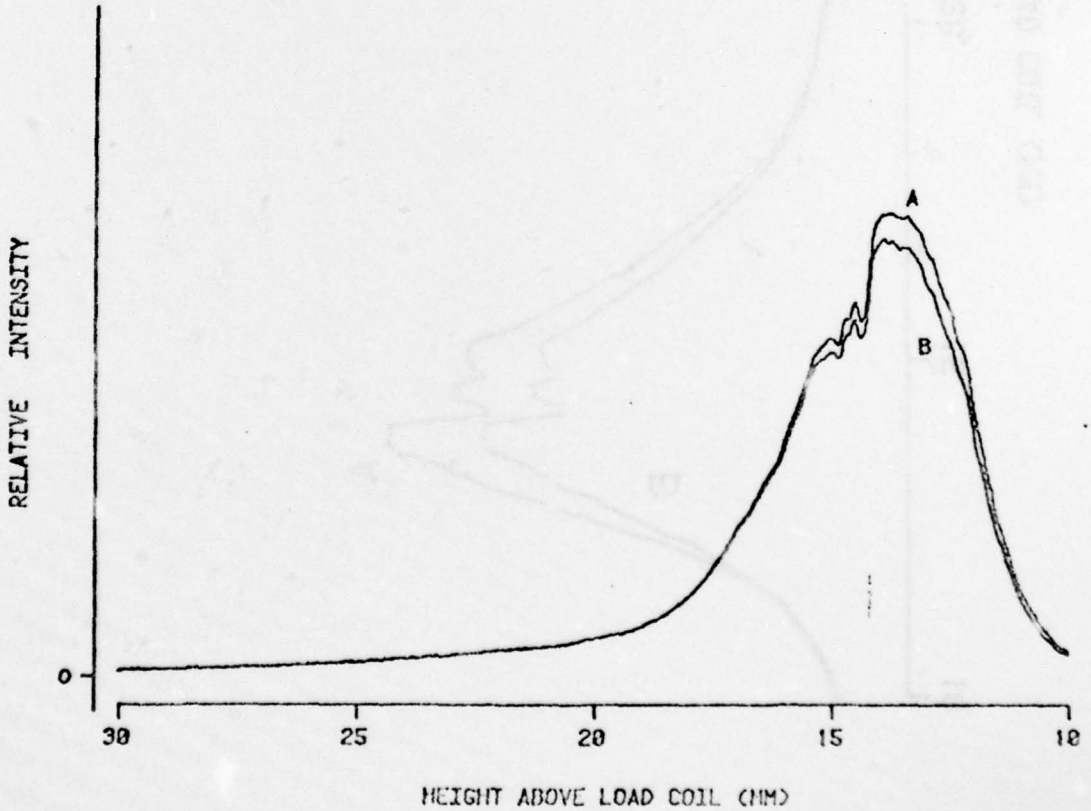
RELATIVE INTENSITY
0
A
B
30
25
20
15
10
HEIGHT ABOVE LOAD COIL (MM)

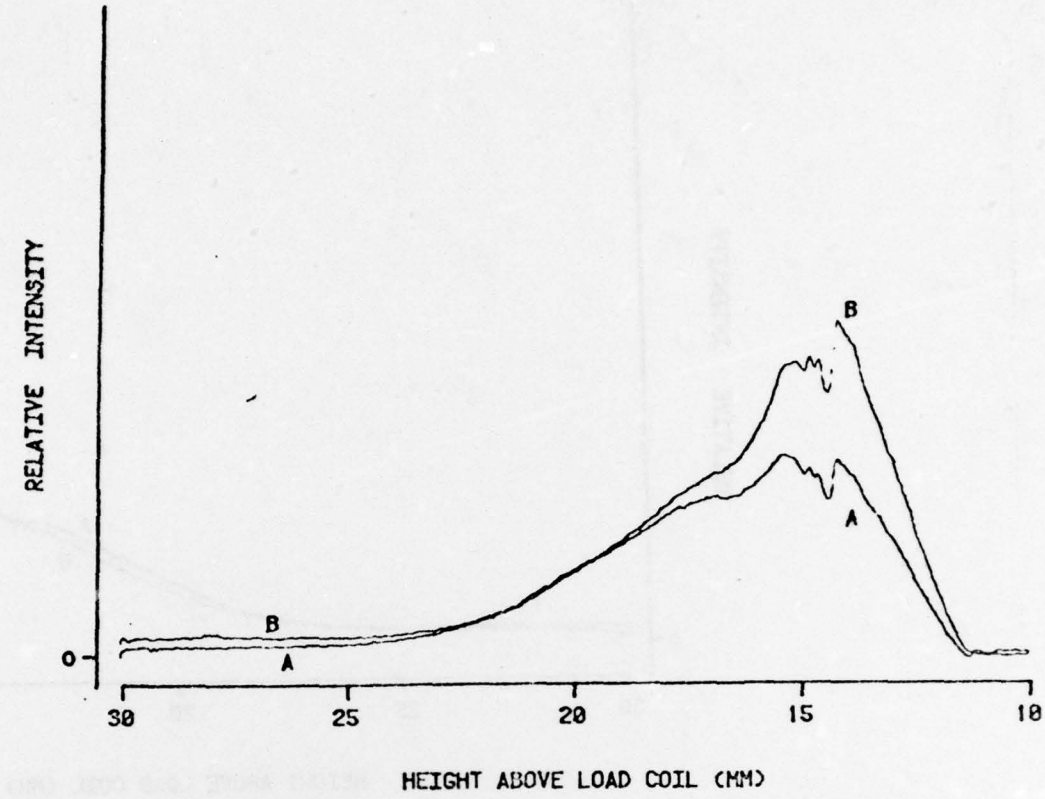
RELATIVE INTENSITY
B
A
B
A
0
30
25
20
15
10
HEIGHT ABOVE LOAD COIL (MM)

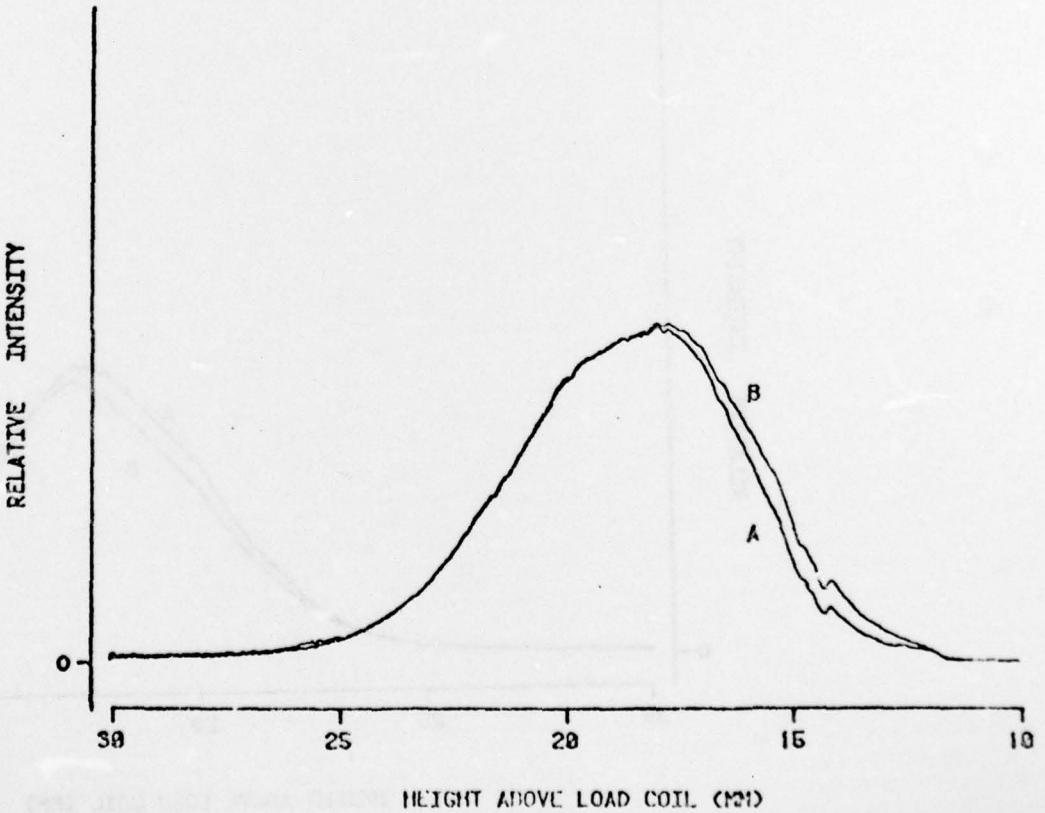
RELATIVE INTENSITY
B
A
0
30
25
20
15
10
HEIGHT ABOVE LOAD COIL (MM)

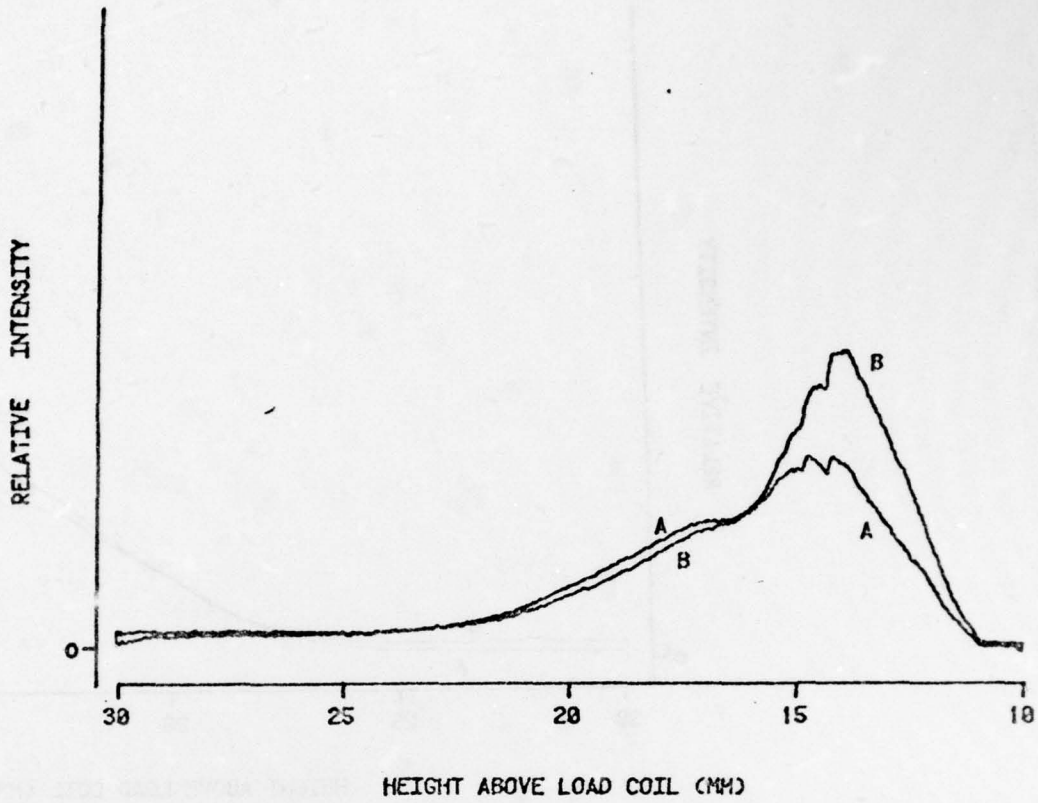
RELATIVE INTENSITY
0
30
25
20
15
10
A
B
B
A
HEIGHT ABOVE LOAD COIL (MM)

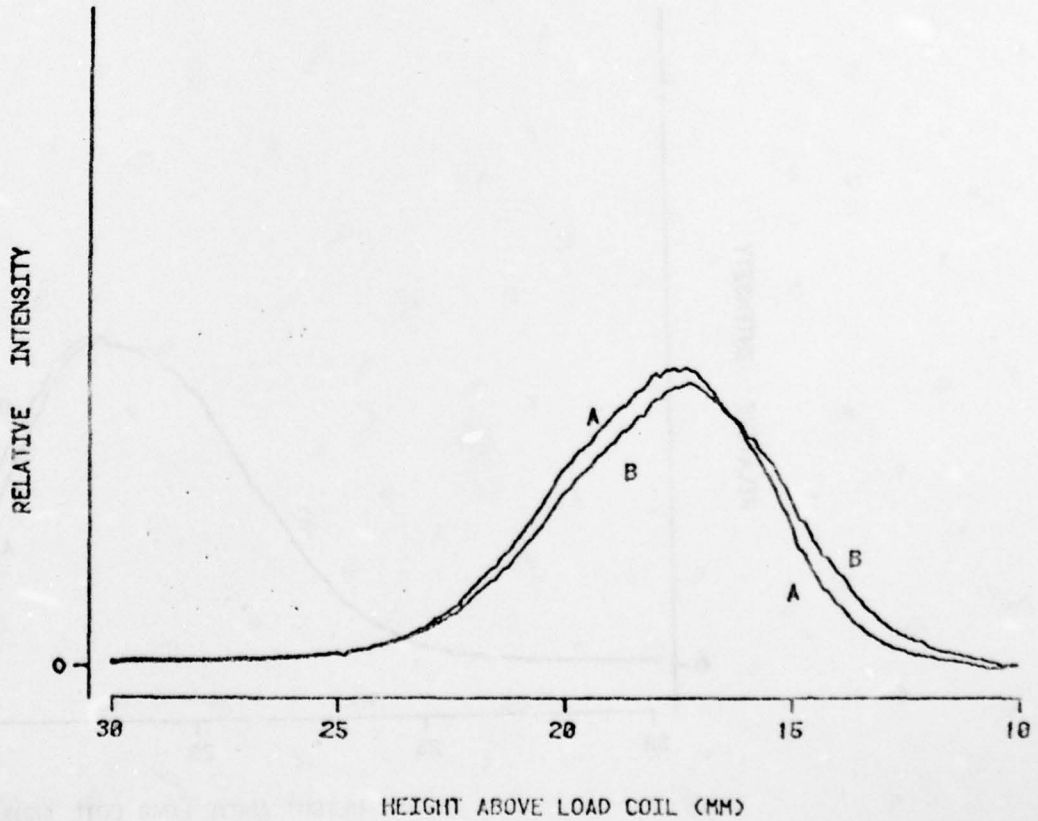
RELATIVE INTENSITY
0
30
25
20
15
10
A
B
B
A
HEIGHT ABOVE LOAD COIL (MM)

TECHNICAL REPORT DISTRIBUTION LIST, GEN

	No. Copies
Office of Naval Research Attn: Code 472 800 North Quincy Street Arlington, Virginia 22217	2
ONR Branch Office Attn: Dr. George Sandoz 536 S. Clark Street Chicago, Illinois 60605	1
ONR Branch Office Attn: Scientific Dept. 715 Broadway New York, New York 10003	1
ONR Branch Office 1030 East Green Street Pasadena, California 91106	1
ONR Branch Office Attn: Dr. L. H. Peebles Building 114, Section D 666 Summer Street Boston, Massachusetts 02210	1
Director, Naval Research Laboratory Attn: Code 6100 Washington, D.C. 20390	1
The Assistant Secretary of the Navy (R,E&S) Department of the Navy Room 4E736, Pentagon Washington, D.C. 20350	1
Commander, Naval Air Systems Command Attn: Code 310C (H. Rosenwasser) Department of the Navy Washington, D.C. 20360	1
Defense Documentation Center Building 5, Cameron Station Alexandria, Virginia 22314	12
Dr. Fred Saalfeld Chemistry Division Naval Research Laboratory Washington, D.C. 20375	1
U.S. Army Research Office Attn: CRD-AA-IP P.O. Box 1211 Research Triangle Park, N.C. 27709	1
Naval Ocean Systems Center Attn: Mr. Joe McCartney San Diego, California 92152	1
Naval Weapons Center Attn: Dr. A. B. Amster, Chemistry Division China Lake, California 93555	1
Naval Civil Engineering Laboratory Attn: Dr. R. W. Drisko Port Hueneme, California 93401	1
Department of Physics & Chemistry Naval Postgraduate School Monterey, California 93940	1
Dr. A. L. Slafkosky Scientific Advisor Commandant of the Marine Corps (Code RD-1) Washington, D.C. 20380	1
Office of Naval Research Attn: Dr. Richard S. Miller 800 N. Quincy Street Arlington, Virginia 22217	1
Naval Ship Research and Development Center Attn: Dr. G. Bosmajian, Applied Chemistry Division Annapolis, Maryland 21401	1
Naval Ocean Systems Center Attn: Dr. S. Yamamoto, Marine Sciences Division San Diego, California 91232	1
Mr. John Boyle Materials Branch Naval Ship Engineering Center Philadelphia, Pennsylvania 19112	1

P4-2/B13

472:GAN:716:1a
78u472-608

TECHNICAL REPORT DISTRIBUTION LIST, 051C

	No. Copies
Dr. M. B. Denton Department of Chemistry University of Arizona Tucson, Arizona 85721	1
Dr. R. A. Osteryoung Department of Chemistry State University of New York at Buffalo Buffalo, New York 14214	1
Dr. B. R. Kowalski Department of Chemistry University of Washington Seattle, Washington 98105	1
Dr. S. P. Perone Department of Chemistry Purdue University Lafayette, Indiana 47907	1
Dr. D. L. Venezky Naval Research Laboratory Code 6130 Washington, D.C. 20375	1
Dr. H. Freiser Department of Chemistry University of Arizona Tuscon, Arizona 85721	
Dr. Fred Saalfeld Naval Research Laboratory Code 6110 Washington, D.C. 20375	1
Dr. H. Chernoff Department of Mathematics Massachusetts Institute of Technology Cambridge, Massachusetts 02139	1
Dr. K. Wilson Department of Chemistry University of California, San Diego La Jolla, California	1
Dr. A. Zirino Naval Undersea Center San Diego, California 92132	1

	No. Copies
Dr. John Duffin United States Naval Postgraduate School Monterey, California 93940	1
Dr. G. M. Hieftje Department of Chemistry Indiana University Bloomington, Indiana 47401	1
Dr. Victor L. Rehn Naval Weapons Center Code 3813 China Lake, California 93555	1
Dr. Christie G. Enke Michigan State University Department of Chemistry East Lansing, Michigan 48824	1
Dr. Kent Eisentraut, MBT Air Force Materials Laboratory Wright-Patterson AFB, Ohio 45433	1
Walter G. Cox, Code 3632 Naval Underwater Systems Center Building 148 Newport, Rhode Island 02840	1
Dr. Rudolph J. Marcus Office of Naval Research Scientific Liaison Group American Embassy APO San Francisco 96503	1
Mr. James Kelley DTNSRDC Code 2803 Annapolis, Maryland 21402	